Japanese Journal of Applied Physics

The Japan Society of Applied Physics

Transmission structural-color characteristics of Al-ZrO_2-SiO_2 plasmonic linear gratings

Japanese Journal of Applied Physics **61**, 092001 (2022) **REGULAR PAPER**
https://doi.org/10.35848/1347-4065/ac8650

Transmission structural-color characteristics of Al-ZrO_2-SiO_2 plasmonic linear gratings

Sangwon Ham[1], Byeong-Kwon Ju[1], and Hwi Kim[2*]

[1] *Display and Nanosystem Laboratory, School of Electrical Engineering, Korea University, Seoul 02841, Republic of Korea*
[2] *Department of Electronics and Information Engineering, Korea University Sejong Campus, Sejong 30019, Republic of Korea*

[*] E-mail: hwikim@korea.ac.kr

Received March 31, 2022; revised July 7, 2022; accepted July 31, 2022; published online August 26, 2022

This paper investigates the color characteristics of Al-ZrO_2-SiO_2 plasmonic linear gratings, particularly focusing on the trade-off between the purity of the surface plasmon resonance induced color and the transmission efficiency. In our proposed plasmonic color filter, the factor that determines the resonance wavelength is the grating period, and the main factor controlling the relationship between color purity and transmittance is the grating fill factor, i.e. duty ratio. This means that the bandwidth of the transmittance spectrum can be tuned using the fill factor. Its physical reasoning is described. A full-color pallet is fabricated in the form of an Al-ZrO_2-SiO_2 linear grating with a fixed thickness and adjusted pairings of the grating period and fill factor.

1. Introduction

Plasmonic structural-color filters are considered a promising technology that can compete with the conventional dye-based color filters.[1–3] Research on the surface plasmonic resonance (SPR) associated with metals such as Ag, Al, Au and Cr has been actively conducted for highly reliable plasmonic color filters (PCFs).[4–6] PCFs composed of a metal dielectric composite have particular attention because of their mechanical strength, low chemical reaction, wavelength-scale footprint, and ultra-high resolution. PCFs offer a wide range of potential applications, including various optical devices such as organic light-emitting diodes, liquid crystal displays, quantum dot displays, and CMOS image sensors.[7–12] PCFs can have various geometric structures and constituent materials and can be utilized as transmission or reflection type filters. Well-known PCF prototypes have been based on planar multilayers, periodic gratings, periodic hole arrays, hole disk arrays or square arrays.[13–16] In almost all PCFs, the SPR-based structural-color is manipulated by geometric factors such as size, period, and layer thickness. Theoretically, the metal dielectric composite can be considered as a coupled resonator of metallic resonator and dielectric resonator. High refractive index materials such as ZrO_2 allows high degree of freedom in the design of PCFs, and in particular, have been widely adopted in PCFs for refining spectral bandwidth and enhancing optical efficiency.[17,18]

In this paper, we investigate a transmission-type PCF with a linear grating structure in the visible band and fabricate a full-color pallet based on Al-ZrO_2-SiO_2 linear gratings. The transmission characteristics of the linear grating PCF and their dependence on the geometrical parameters of the grating are analyzed with both numerical simulations and experiments. Various figures of merit for color-purity performance, including the color gamut, angular sensitivity, and color purity (i.e. spectral bandwidth) have been developed in past studies,[19–22] but, in this paper, we mainly focus on the trade-off relationship between the spectral bandwidth and transmission efficiency according to the adjustment of the structural parameters of PCF. In the fabrication of the full-color pallet, the grating thickness is assumed to be fixed for the PCF color pallet to minimize the fabrication complexity and thus ensure the manufacturability of the proposed design.

This paper is structured as follows. In Sect. 2, the analysis of the ZrO_2 dielectric layer for improving the color purity of the proposed PCF is presented. In Sect. 3, the design of the proposed PCF and the numerical analysis of its color characteristics are presented and Sect. 4 describes a discussion about the influence of fill factor on transmission characteristics of the PCF. Finally, the fabrication of the PCF color pallet and the results of the subsequent experiments are presented in Sect. 5. Based on the simulation, fabrication and experimental assessment of the PCF color pallet, a conclusion about the relationship between the color gamut variation and transmission efficiency associated with the grating period and fill factor is provided.

2. High refractive index waveguide for high color purity

An extraordinary optical transmission phenomenon, in which the transmittance is improved by the coupling of light with plasmon, is observed in the periodically patterned metallic structure.[23] In order to improve the transmittance efficiency and color filter characteristics within the visible band, the dual-layer structure of a metallic grating and a dielectric layer is employed. Figure 1 shows the filter characteristics that change depending on the presence or absence of metallic grating and ZrO_2 layer. The Al grating and the SiO_2 substrate can be considered as a single optical resonator. The single Al grating without the ZrO_2 dielectric layer is a single optical resonator boosted by surface plasmon. Figure 1(a) shows a metallic grating structure that transmits light waves of 532 nm wavelength in the visible region. The transmission spectrum is plotted by the dotted curve in Fig. 1(c), which presents a broad full width at half maximum (FWHM) spectrum around 300 nm wavelength. The single dielectric layer is a waveguide resonator with single or multimodal resonances, i.e. guided mode resonance.

The dual-layer structure of the Al grating and ZrO_2 dielectric layer can be seen as a coupled resonator creating a transmission resonance profile that cannot be obtained by a single Al grating or a single ZrO_2 dielectric layer. The surface plasmon resonance mode and the guided mode resonance are combined to coupled resonance modes. We can obtain an improved tunability in resonance wavelength and spectral profile.

Figure 1(b) presents the resonance field distribution in the dual-layer structure at 532 nm wavelength. Its transmission

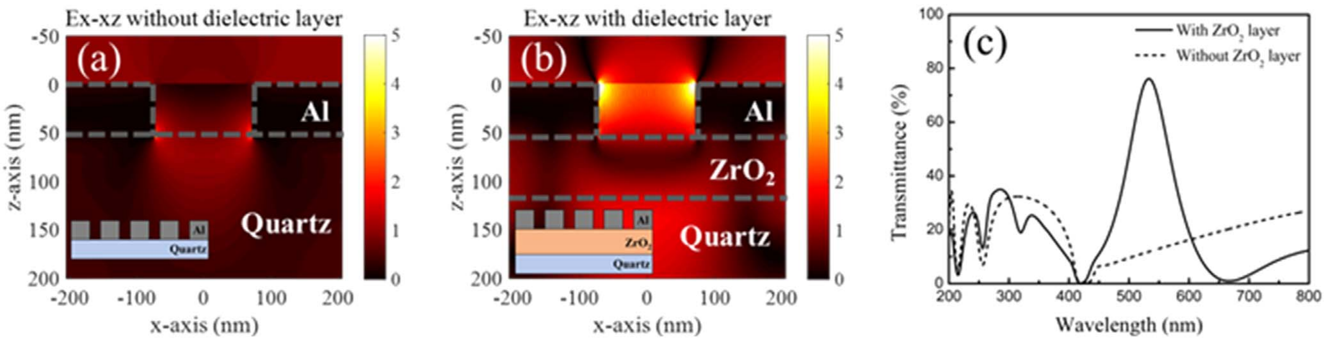

Fig. 1. (Color online) Characteristics of PCF by high refractive index ($n_{ZrO2} = 2.17$ at wavelength 532 nm) layer. Distribution of cross-section electric field of metallic grating PCF (a) without high refractive index layer and (b) high refractive layer PCF surrounded by metallic grating and substrate. (grating period = 410 nm, fill factor = 0.65, metal (Al) layer thickness = 55 nm, dielectric (ZrO_2) layer thickness = 65 nm, wavelength = 532 nm). (c) Transmittance spectrums with and without ZrO_2 waveguide layer.

spectrum is plotted by the solid line curve in Fig. 1(c). The resonance center wavelength is positioned at 532 nm green color and the transmission efficiency is highly improved. The matching of SPR mode and guided mode resonance in a structure composed of metallic grating and dielectric causes a strong field, showing high transmittance. The coupled resonator structure is widely used in various applications.

The relatively high refractive index dielectric layer helps to narrow the transmission bandwidth in the structural-color filter application because the high refractive index dielectric waveguide has more sensitive dispersion relation in its propagation constant of guided mode. That means a little wavelength change leads to relative larger change in the propagation constant in the high refractive index waveguide rather than in low refractive index waveguide.

3. PCF design and numerical simulations

The target template structure for the plasmonic linear grating is presented in Fig. 2(a). The layered structure is composed of an Al linear grating (height h_1, period Λ, and width of Al line w) and a ZrO_2 dielectric layer with a refractive index of 2.17 and thickness h_2 on a finite-thickness quartz substrate. The grating fill factor is defined by the ratio w/Λ. In the construction of the visible band color pallet, h_1 and h_2 are assumed to be fixed for the entire color gamut to simplify the manufacturing process and produce PCF gratings that express various colors with a single thickness layer. Consequently, grating period and fill factor are set to main design parameters that will be optimized.

The PCF grating in Fig. 2(a) is assumed to have fixed thickness h_1 of 55 and h_2 of 65 nm. Using the fill factor of 0.65, the structural conditions required to produce the three primary colors, red (625 nm), green (535 nm) and blue (465 nm) can be identified. The resonance wavelength for each color is mainly determined by the grating period. The grating period for red, green, and blue PCFs are found to be $\Lambda_R = 530$ nm, $\Lambda_G = 410$ nm, and $\Lambda_B = 315$ nm, respectively. In a linear grating structure, the coloration effect is sensitive to the polarization of the illuminating light because the SPR is selectively induced by transverse magnetic (TM) polarization. The TM-polarized light passes through the PCF grating to generate coloration effect, while the Al grating layer is highly reflective to the transverse electric polarized light. The Al layer thus acts as a wire grid polarizer.

For the computational electromagnetic analysis, the Fourier modal method (FMM) is employed.[24] The FMM is the frequency domain method for electromagnetic analysis based on the scattering matrix (S-matrix) method, that is a theory of modeling optical multi-block structures with forward and backward wave-propagation operators. A numerical simulation of the red PCF structure with Λ of 530 nm under TM mode illumination with a wavelength of 625 nm is presented in Fig. 2(b). SPR is observed in the resulting electric field distribution within a single period unit.

In the dual-layer PCF structure, the incident light diffracted by the Al grating is coupled into the optical modes of a ZrO_2 waveguide, propagating along the x-axis, and combined with a strongly enhanced SPR field to efficiently transmit light. Figure 2(c) presents the transmittance spectrum for the primary colors generated by the designed PCF gratings ($\Lambda_R = 530$ nm, $\Lambda_G = 410$ nm, and $\Lambda_B = 315$ nm). In the transmittance spectrum for red, green, and blue, the maximum transmittance is 75.3%, 76.3% and 69.0%, respectively, while the FWHM is 92.5 nm, 90.0 nm and 79.5 nm, respectively. In Fig. 2(d), the colors corresponding to the transmittance spectrum of the designed red, green and blue structures are indicated in a CIE chromaticity diagram. The obtained color gamut is relatively limited compared to that of the ideal red, green, and blue primary colors, but it is identified that the fill factor can be used to effectively enhance the color gamut.

Figure 3 presents three designs for the PCF color representing the full-color characteristics for a fill factor of 0.5, 0.6, and 0.7. In Fig. 3(a), the transmittance spectrum is simulated in the range of the grating period varying from 250 to 550 nm, with a sampling interval of 20 nm. It can be observed that the resonance wavelength increases proportionally with the grating period within this range, with a total wavelength shift of 225 nm. The transmittance spectrums are plotted for fill factors of 0.5, 0.6, and 0.7. The fill factor directly affects the FWHM. When the fill factor is increased from 0.5 to 0.7 for the same period, the resonance wavelength exhibits red shift and the bandwidth of the PCF tends to be narrow. In Fig. 3(b), therefore, the color purity of the PCF varies with the fill factor, which is represented by the variation in the diameter of the color-traces in the CIE chromaticity diagram. As shown in Fig. 3(c), A fill factor of 0.7 produces the widest color gamut compared to 0.5 and 0.6 fill factors.

The colors corresponding to the resonant wavelengths of transmitted light complete a closed loop in the CIE chromaticity diagram. In Fig. 3(b), the observed color is expressed in

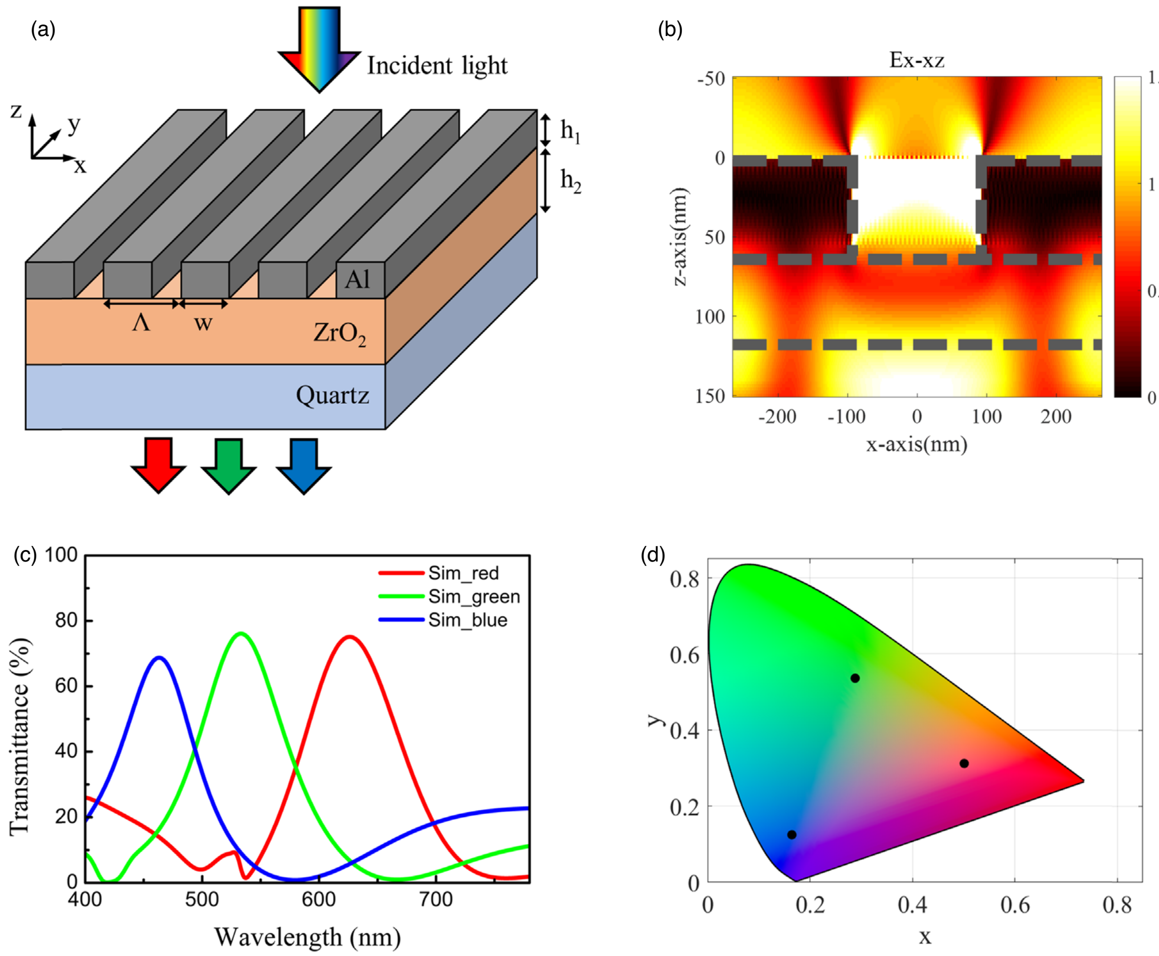

Fig. 2. (Color online) (a) Schematic geometry of a 1D grating plasmonic color filter (PCF). (b) Electric field distribution in the *x–z* cross-section. (c) Transmittance spectrum of the PCFs for red (633 nm, red line), green (532 nm, green line) and blue (475 nm, blue line) colors. (d) Color coordinates on a CIE chromaticity diagram for the red, green, and blue structures.

the CIE color coordinate system for fill factors of 0.5, 0.6, 0.7 and the grating periods from 250 to 550 nm in 10 nm steps. In the CIE chromaticity diagram, the color-traces for the PCF are plotted for pairs of the pairing of grating period and fill factor. The color traces exhibit different pathways in the diagram according to the fill factor. In the color coordinate system with a fill factor of 0.7, 250 nm period starts in the blue region (0.3102, 0.1445) and moves counterclockwise to the red region (0.4456, 0.2381) for a 550 nm period. As the fill factor decreases, the range of colors tends to shrink.

In Fig. 3(c), for all the visible colors, the transmittance is inversely proportional to the fill factor. The overall transmittance for a fill factor of 0.5 ranges from 69% to 86%, which is larger than that for the fill factors of 0.6 and 0.7. Figure 3(c) shows that there is no significant difference in the FWHM between the fill factors above the period of 500 nm. The FWHM moves from 61 to 88 nm for the fill factor of 0.7, while it increases from 100 to 150 nm for a fill factor of 0.5. The difference in the FWHM is conspicuous in the blue PCF with periods smaller than 350 nm. Based on the analysis of Figs. 3(b) and 3(c), the color pallet represented by the CIE diagram in Fig. 3(b) can be constructed using the PCFs with a 65 nm thick ZrO_2 layer and a 55 nm thick Al grating, thus identifying a PCF design that satisfies the given specification of FWHM (color purity).

4. Analysis of the relationship between transmittance and FWHM dependent on fill factor

The Al-ZrO_2-SiO_2 plasmonic linear gratings structure can control full-color, color purity, and transmittance by the period and fill factor of metallic grating. The effect of Al grating fill factor on transmittance and bandwidth is explained based on an effective medium determined by air and metal. Air has the same permittivity of 1 over the entire wavelength range, while Al (metal) is dispersive to wavelength. Therefore, as an effective medium, the 1D Al grating responds more sensitively to wavelength change around resonance conditions as the metal occupancy i.e. fill factor, increases. In Fig. 4(a), the strong dispersive Al grating with high fill factor shows narrower transmission spectral profile because it is easier to deviate from the resonance condition at a specific wavelength, while the weak dispersive Al grating with low fill factor shows a transmission spectral profile with relatively wider FWHM because, the detuning due to the refractive index change of the Al-air effective medium is relatively weak. As shown in Fig. 3, this property is consistently observed when the Al grating and ZrO_2 layer comprise a dual-layer structure. The dispersion strength of the Al grating associated with the fill factor causes the trade-off relationship between the transmittance and FWHM. In

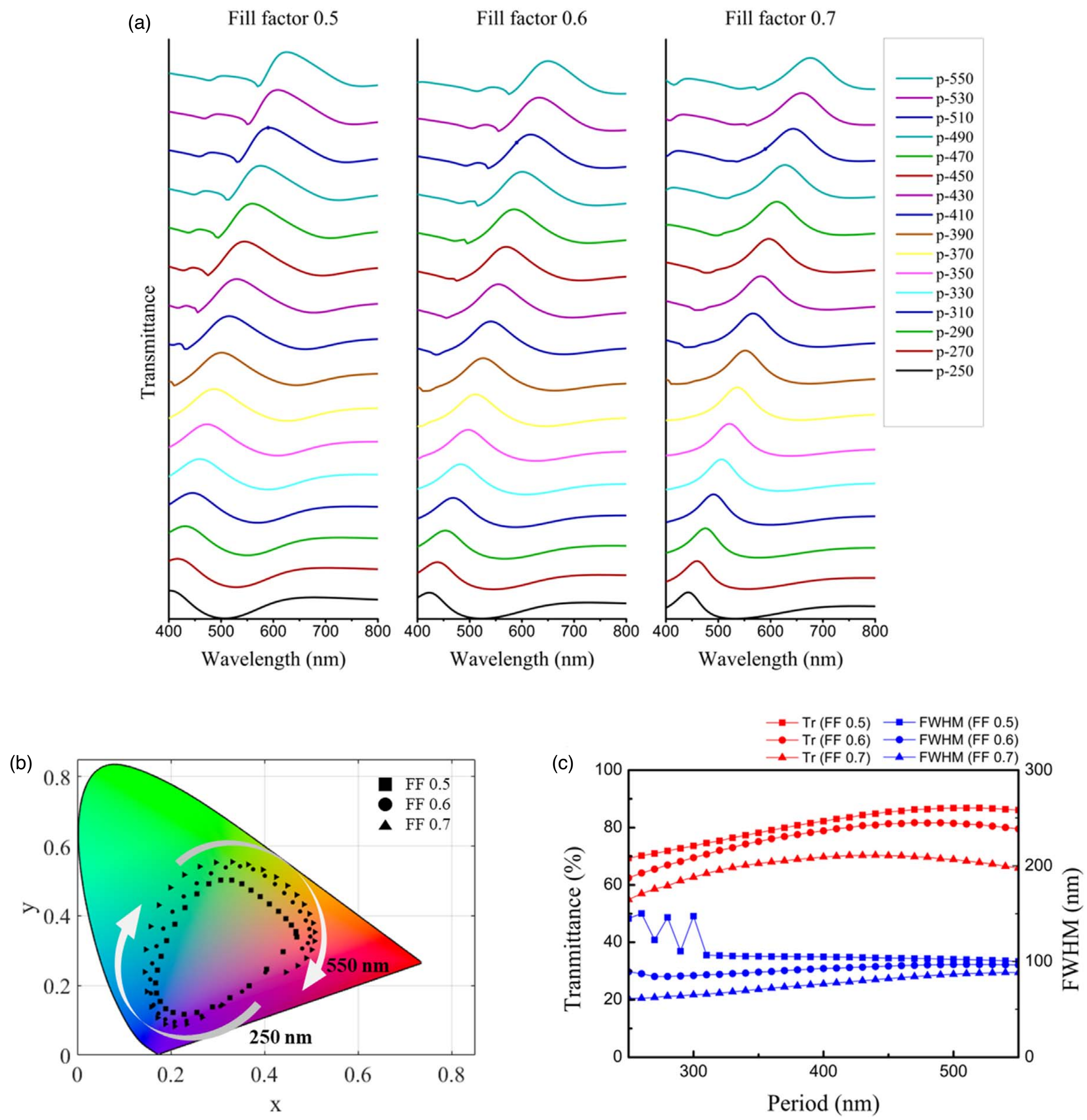

Fig. 3. (Color online) Optical properties of 1D grating PCFs with grating period from 250 to 550 nm and fill factors of 0.5, 0.6, and 0.7. (a) Transmittance spectrum, (b) CIE chromaticity diagram according to period and fill factor, and (c) maximum transmittance at the resonance wavelength and FWHM depending on the period.

Figs. 4(b)–4(d), the electric field distributions formed inside the structure are presented for the wavelength $\lambda_c = 532$ nm and the wavelengths shifted by ±50 nm from the center wavelength. It is shown that the electric field strength is lowered away from the center wavelength. The higher fill factor with strong dispersive Al grating will show more abrupt change in the field intensity and a decreased total transmission efficiency.

We can further develop more intuitive understanding of the trade-off relationship in Figs. 4(e) and 4(f). Under the SPR condition $\lambda = \lambda_c$, the electric field is strongly focused at the center of slit and, at a detuning condition $\lambda = \lambda_c + \Delta\lambda_1$, the focused electric field is slightly spread. Furthermore, at $\lambda = \lambda_c + \Delta\lambda_2$, a further spread is expected in the electric field distribution as illustrated in Fig. 4(e), where $\Delta\lambda_1 < \Delta\lambda_2$. The transmission efficiencies for $\lambda = \lambda_c$, $\lambda = \lambda_c + \Delta\lambda_1$ and $\lambda = \lambda_c + \Delta\lambda_2$ are highly dependent on the slit width. The figure-of-merit of the transmission energy is approximately modeled by an overlap integral of the electric field profile, then for a wide aperture slit with small fill factor, the difference in the transmission energy for the three cases would be small, while for a narrow aperture slit with large fill factor, the difference in the transmission efficiency would be large. The normalized transmission efficiency is plotted as a function of the operating wavelength and the fill factor in Fig. 4(f). The former case (large fill factor) generates relatively wider FWHM transmission spectrum, while the latter case (small fill factor) generates relatively narrower FWHM transmission spectrum.

5. Experimental results

In this section, the PCF color pallet designed in Sect. 3 is fabricated and experimentally tested. Figure 4 presents the fabricated color pallet of 3×13 PCFs consisting of 55 nm thick Al gratings, of which the period varied, and a 65 nm thick ZrO_2 layer on a quartz substrate. The first step in

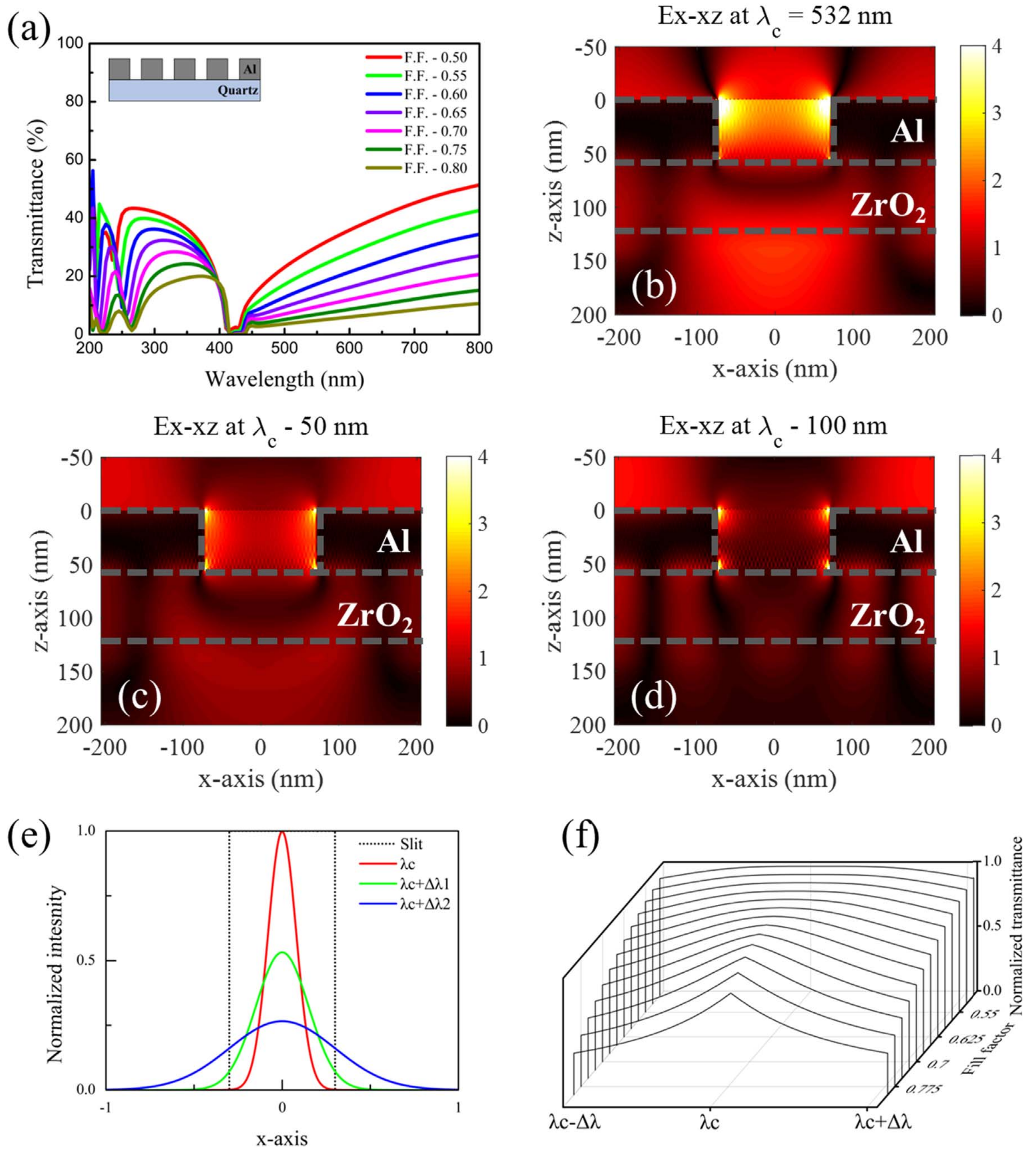

Fig. 4. (Color online) Optical properties of PCF dependent on multiple fill factors. (a) Al grating transmittance spectrum dependent on fill factor from 0.5 to 0.8. Electric field distributions of the PCF cross-section at the operating wavelengths (b) $\lambda_c = 532$ nm, (c) $\lambda_c - 50$ nm, and (d) $\lambda_c - 100$ nm. (e) The intensity profile of the field transmits the finite width slit structure. (f) The normalized transmittance affected by the fill factor at the center wavelength (λ_c) and shifted wavelength ($\lambda_c \pm \Delta\lambda$).

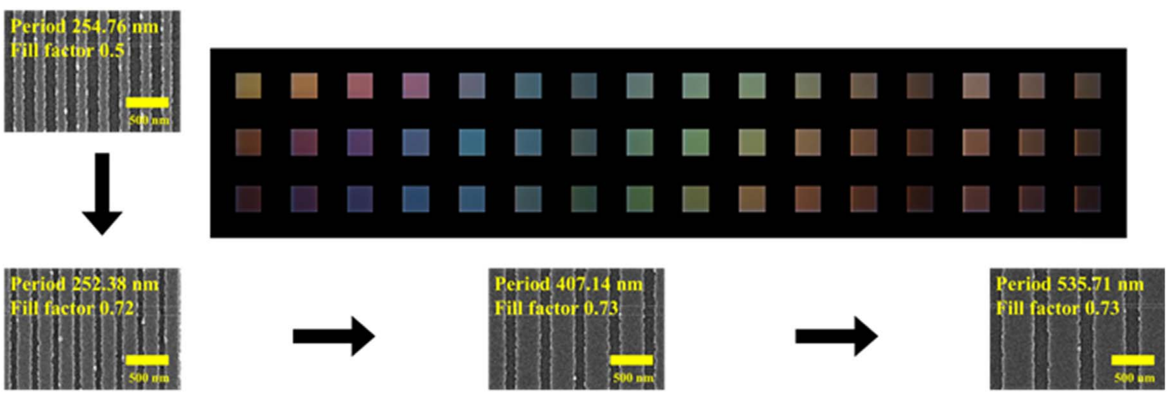

Fig. 5. (Color online) Optical micro-photographs of 1D grating PCFs with a grating period from 250 to 550 nm and fill factors of 0.5, 0.6, and 0.7. SEM images of the fabricated device with target fill factors 0.5 and 0.7 and the target period increasing from 250 to 530 nm (scale bar: 500 nm).

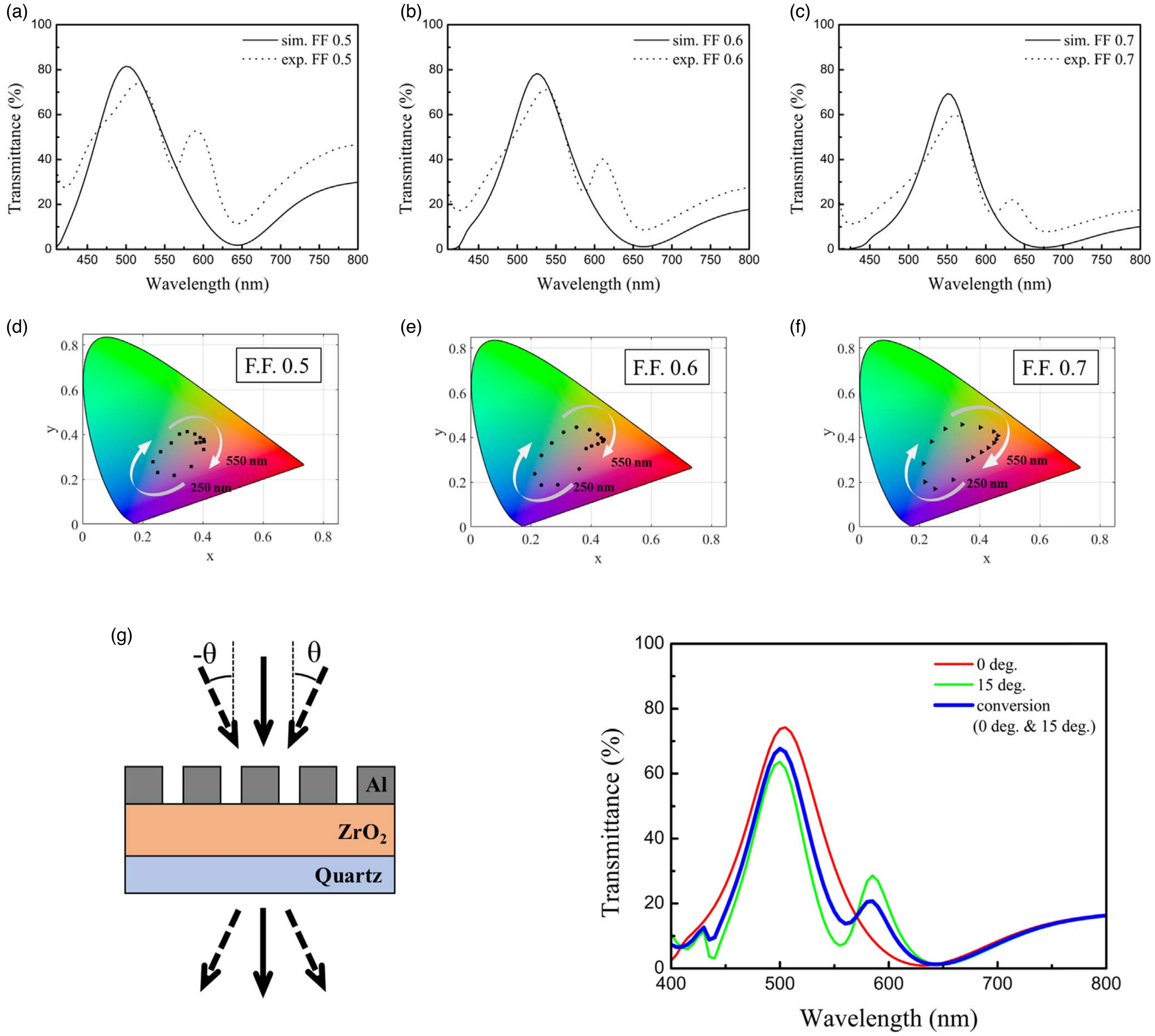

Fig. 6. (Color online) Experimentally measured optical properties of a 1D grating PCF for various filter and periods. Transmittance spectrum for fill factors (a) 0.5, (b) 0.6, and (c) 0.7 with a grating period of 390 nm (the dashed line represents the experimental results, while the solid line represents the simulation results). CIE chromaticity diagram for fill factors (d) 0.5, (e) 0.6, and (f) 0.7 for structures with a grating period from 250 to 550 nm. (g) Secondary peak dependent on incident angle (black line is normal incidence, black dotted line is the incident beam tilted by 15 degrees, red dotted line is average transmittance).

fabricating the PCF pallet is a deposition of a 65 nm thick ZrO_2 layer on a 0.5 mm Eagle XG glass (Corning) substrate using atomic layer deposition. The second step is thermal evaporation of a 55 nm thick Al layer and subsequent patterning of periodic Al gratings using e-beam lithography (JBX-9300FS, JEOL). Finally, Al pattern etching was conducted using inductive coupling plasma reactive ion etching (ICP-RIE) with Cl_2 gas. Figure 5 presents optical microscope image taken under TM polarized backside white-light illumination for the PCF gratings with a grating period from 250 to 550 nm in 20 nm interval and grating fill factors of 0.5, 0.6, and 0.7, showing their own colors. In the SEM image, the error of the target grating period of the fabricated device was analyzed. There is an error of 0.19% and 0.01% in 250 nm target device, 0.7% error in 410 nm target device, and 1.1% error in 530 nm target device. Considering that a 1 nm increase in the grating period shifts the resonance wavelength by 0.78 nm, it could be said that an error of less than 1% is within the allowable range.

To experimentally observe the relationship between the fill factor and the FWHM, the transmittance spectrum of the PCFs with a period of 390 nm and three fill factors are measured and compared in Figs. 6(a)–6(c). The dotted curves indicate the experimentally measured spectrum, while the solid curves are those obtained by the numerical simulation. The resonance wavelength of the measured transmittance spectrum is 515 nm, 535 nm and 560 nm, for a fill factor of 0.5, 0.6, and 0.7, respectively; compared with the simulation results, the experimental results exhibit a red shift of 15 nm, 10 nm, and 10 nm, respectively. The PCFs for the fill factors of 0.5, 0.6 and 0.7 record the maximum transmittances of 74.0%, 71.2% and

59.9%, respectively at those resonance wavelengths. As illustrated in Fig. 2, the tendency that the transmittance decreases with an increase in the fill factor is clearly observed. Compared with the calculated maximum transmittance, the experimental values for the fill factors of 0.5, 0.6 and 0.7 were reduced by 7.2%, 7.1%, and 9.4%, respectively. This deviation can be ascribed to fabrication errors in the color pallet sample. Unintended secondary peak in each measured transmittance spectrum is observed in the wavelength range of 590–635 nm. Those secondary peaks are not observed in the numerical simulation data. This unwanted secondary peak appears to originate from multiplex reflections in the finite size quartz substrate. Therefore, as shown in Figs. 6(d)–6(f), the intended green color tends to shift in the red direction in the CIE chromaticity diagram. The PCFs with a higher fill factor (0.7) are more effective in suppressing the red-shifted secondary resonance than those with the lower fill factor (0.5). The area expressed in the CIE chromaticity diagram represents the color gamut of the fabricated PCF pallet. The experimental results find that the color gamut increases with an increase in the fill factor. The experimental data in the CIE chromaticity diagram thus agrees with the simulation data for the color gamut presented in Fig. 3(b).

Experiments present a secondary peak generation at around 600 nm wavelength. We investigated several causes. The oxide layer grown on the Al top side,[25] the ZrO_2 and SiO_2 composite interface synthesized at high temperature,[26] and the oblique incidence of illumination light can be the suitable causes. From various investigations, we conclude that secondary peaks can arise by oblique incidence component of the illuminating light. In Fig. 6(g), it shows that a secondary peak is generated in the transmission spectrum under converging illumination with a −15 to +15 deg oblique incident component, which is the same phenomenon shown in Figs. 6(a)–6(c). Consequently, we find that the secondary peak was caused by the use of the convergence LED illumination instead of a perfectly collimated laser beam.

6. Conclusion

In conclusion, we have designed and fabricated a 3×13 visible band PCF color pallet composed of Al-ZrO_2-SiO_2 plasmonic linear gratings on a single substrate that produces red, green, and blue primary colors and experimentally demonstrated that the fill factor affects the color purity and transmittance efficiency. Because an increase in the fill factor leads to an enhancement in the color purity and color gamut at the cost of transmission efficiency, and a balance is required in the design of a PCF to meet performance specifications. The relationship between transmittance and FWHM affected by the fill factor was verified through theoretical and experimental analysis.

Acknowledgments

This work was supported by Institute of Information & Communications Technology Planning & Evaluation (IITP) Grant funded by the Korean government (MSIT) [No. 2020-0-00914, Development of hologram printing downsizing technology based on holographic optical element (HOE)].

1) F. Cheng, J. Gao, T. S. Luk, and X. D. Yang, "Structural color printing based on plasmonic metasurfaces of perfect light absorption," Sci. Rep. **5**, 11045 (2015).
2) V. R. Shrestha, S. S. Lee, E. S. Kim, and D. Y. Choi, "Non-iridescent transmissive structural color filter featuring highly efficient transmission and high excitation purity," Sci. Rep. **4**, 4921 (2014).
3) H. S. Lee, Y. T. Yoon, S. S. Lee, S. H. Kim, and K. D. Lee, "Color filter based on a subwavelength patterned metal grating," Opt. Express **15**, 15457 (2007).
4) Y. Ye, Y. Zhou, and L. S. Chen, "Color filter based on a two-dimensional submicrometer metal grating," Appl. Opt. **48**, 5035 (2009).
5) X. L. Hu et al., "Influence of film thickness and nanograting period on color-filter behaviors of plasmonic metal Ag films," J. Appl. Phys. **115**, 113104 (2014).
6) G. Y. Si, Y. H. Zhao, H. Liu, S. Teo, M. S. Zhang, T. J. Huang, A. J. Danner, and J. H. Teng, "Annular aperture array based color filter," Appl. Phys. Lett. **99**, 033105 (2011).
7) Y. Cho, Y. K. Choi, and S. H. Sohn, "Optical properties of neodymium-containing polymethylmethacrylate films for the organic light emitting diode color filter," Appl. Phys. Lett. **89**, 051102 (2006).
8) S. Yokogawa, S. P. Burgos, and H. A. Atwater, "Plasmonic color filters for CMOS image sensor applications," Nano Lett. **12**, 4349 (2012).
9) Q. Chen, D. Chitnis, K. Walls, T. D. Drysdale, S. Collins, and D. R. S. Cumming, "CMOS photodetectors integrated with plasmonic color filters," IEEE Photon. Technol. Lett. **24**, 197 (2012).
10) Y. Yu, Q. Chen, L. Wen, X. Hu, and H. F. Zhang, "Spatial optical crosstalk in CMOS image sensors integrated with plasmonic color filters," Opt. Express **23**, 21994 (2015).
11) K. Matsushima and N. Sonobe, "Full-color digitized holography for large-scale holographic 3D imaging of physical and nonphysical objects," Appl. Opt. **57**, A150 (2018).
12) Y. Tsuchiyama and K. Matsushima, "Full-color large-scaled computer-generated holograms using RGB color filters," Opt. Express **25**, 2016 (2017).
13) A. Ghobadi, H. Hajian, M. C. Soydan, B. Butun, and E. Ozbay, "Lithography-free planar band-pass reflective color filter using a series connection of cavities," Sci. Rep. **9**, 290 (2019).
14) W. Yue, S. Gao, S. S. Lee, E. S. Kim, and D. Y. Choi, "Subtractive color filters based on a silicon-aluminum hybrid-nanodisk metasurface enabling enhanced color purity," Sci. Rep. **6**, 29756 (2016).
15) C. Y. Yang, L. Hong, W. D. Shen, Y. G. Zhang, X. Liu, and H. Y. Zhen, "Design of reflective color filters with high angular tolerance by particle swarm optimization method," Opt. Express **21**, 9315 (2013).
16) Y. S. Do, J. H. Park, B. Y. Hwang, S. M. Lee, B. K. Ju, and K. C. Choi, "Plasmonic color filter and its fabrication for large-area applications," Adv. Opt. Mater. **1**, 133 (2013).
17) K. T. Lee, S. Y. Han, Z. Li, H. W. Baac, and H. J. Park, "Flexible high-color-purity structural color filters based on a higher-order optical resonance suppression," Sci. Rep. **9**, 14917 (2019).
18) C. S. Park, V. R. Shrestha, S. S. Lee, and D. Y. Choi, "Trans-reflective color filters based on a phase compensated etalon enabling adjustable color saturation," Sci. Rep. **6**, 25496 (2016).
19) G. Y. Si et al., "Reflective plasmonic color filters based on lithographically patterned silver nanorod arrays," Nanoscale **5**, 6243 (2013).
20) S. U. Lee and B. K. Ju, "Wide-gamut plasmonic color filters using a complementary design method," Sci. Rep. **7**, 40649 (2017).
21) Y. K. R. Wu, A. E. Hollowell, C. Zhang, and L. J. Guo, "Angle-Insensitive structural colours based on metallic nanocavities and coloured pixels beyond the diffraction limit," Sci. Rep. **3**, 1194 (2013).
22) M. Ye et al., "Angle-insensitive plasmonic color filters with randomly distributed silver nanodisks," Opt. Lett. **40**, 4979 (2015).
23) T. W. Ebbesen, H. J. Lezec, H. F. Ghaemi, T. Thio, and P. A. Wolff, "Extraordinary optical transmission through sub-wavelength hole arrays," Nature **391**, 667 (1998).
24) H. Kim, J. Park, and B. Lee, *Fourier Modal Method and Its Applications in Computational Nanophotonics* (CRC Press, Boca Raton, FL, 2012).
25) S. H. Zaidi, D. W. Reicher, B. L. Draper, J. R. McNeil, and S. R. J. Brueck, "Characterization of thin Al films using grating coupling to surface plasma waves," J. Appl. Phys. **71**, 6039 (1992).
26) G. B. Rayner, D. Kang, Y. Zhang, and G. Lucovsky, "Nonlinear composition dependence of X-ray photoelectron spectroscopy and Auger electron spectroscopy features in plasma-deposited zirconium silicate alloy thin films," J. Vac. Sci. Technol. B **20**, 1748 (2002).